RSC Advances

PAPER

View Article Online
View Journal | View Issue

Cite this: *RSC Adv.*, 2020, **10**, 4805

Study on antibacterial properties and cytocompatibility of EPL coated 3D printed PCL/HA composite scaffolds

Lijiao Tian,[ab] Zhenting Zhang,[a] Bin Tian,[a] Xin Zhang[b] and Na Wang*[a]

Biomaterial scaffolds play a critical role in bone tissue engineering. Moreover, 3D printing technology has enormous advantage in the manufacture of bioengineering scaffolds for patient-specific bone defect treatments. In order to provide an aseptic environment for bone regeneration, ε-poly-L-lysine (EPL), an antimicrobic cationic polypeptide, was used for surface modification of 3D printed polycaprolactone/hydroxyapatite (PCL/HA) scaffolds which were fabricated by fused deposition modeling (FDM) technology. The scaffold morphology and micro-structure were characterized by scanning electron microscopy (SEM), X-ray diffraction (XRD) and transform infrared spectroscopy (FT-IR). The release profile surface roughness, open porosity, and mechanical properties of the scaffolds were evaluated. Cell adhesion, proliferation, differentiation potential and antibacterial properties were also examined. As a result, 3D printed PCL/HA scaffolds with interconnected pores showed a slightly rough surface and improved mechanical properties due to adding hydroxyapatite (HA) particles. After being modified by EPL, favorable biocompatibility and osteoconductivity of ε-poly-L-lysine/polycaprolactone/hydroxyapatite (EPL/PCL/HA) scaffolds were observed. Moreover, antibacterial activity of the EPL/PCL/HA scaffolds was apparent. As a consequence, the EPL/PCL/HA scaffolds had great potential for bone regeneration and prevention of infections. This would yield a patient-specific bioactive and antibacterial composite scaffold for advanced bone tissue engineering applications.

Received 7th December 2019
Accepted 19th January 2020

DOI: 10.1039/c9ra10275b

rsc.li/rsc-advances

1. Introduction

Bone defect is a common disease. Although autologous bone grafting has been the gold standard of bone replacement for many years,[1] its complications, like secondary injury of donor site as well as early and late infection in the post-surgery period, always bring patients more pain and cause the failure of surgery.[2–4] Bone tissue engineering provides a new route for the therapy of bone defects. The scaffolds for bone tissue engineering must have pores interconnected in three dimensions, with highly regular pore formation and structure. The porous structure provides space for cell migration, adhesion, and the ingrowth of new bone tissue. Scaffolds for bone tissue engineering should have reasonable strength and bioactivity, without causing any adverse effects.[5,6]

Rapid prototyping (RP) is one of the most promising techniques for designing and producing three-dimensional (3D) porous scaffolds for cell ingrowth.[7] Compared with conventional polymer processing techniques, such as salt leaching, gas foaming, solvent casting and phase separation, RP can be easily used to fabricate scaffolds with controllable and reproducible porosity,[8,9] offering patients with the exact dimension of individual artificial bone substitute. Fused deposition modeling (FDM), a rapid prototyping technology, is investigated and successfully applied in many research studies to produce novel 3D scaffolds with fully interconnected channel networks, and highly controllable porosity and channel size.[10]

Polycaprolactone (PCL), bioresorbable aliphatic polyester, is a suitable material for cell attachment and proliferation, its degradation by-products are nontoxic and are usually metabolized and eliminated *via* natural pathways.[11,12] As thermoplastic polymers, PCL can easily be processed into three-dimensional (3D) scaffolds with desired geometry and controlled porosity with interconnectivity using modern computer-based solid free-form fabrication methods.[13] However, when used in bone tissue engineering, PCL lacks bioactivity, and the hydrolysis of polyesters exposes carboxylic acid moieties to the local biological environment, known to have caused bone resorption in the past.[14,15]

Materials for bone defect replacement and repairing process should satisfy characteristics of mechanical capacity for bone-bearing, good biocompatibility, osteoconductivity and osteoinductivity. Hydroxyapatite (HA), the main component of natural bone matrix, has drawn wide attention due to its osteoconductive and osteoinductive properties, bone bonding abilities, and slow degradation *in situ*.[16] However, HA has very low

[a]*Beijing Stomatological Hospital, School of Stomatology, Capital Medical University, Beijing 100010, PR China. E-mail: nawangkq@yahoo.com*
[b]*Liangxiang Hospital of Beijing Fangshan District, Beijing 100010, PR China*

tensile strength and is brittle.[17] Therefore, the application of polymeric scaffolds and ceramic particles has shown promising improvements, extending their application as bone patch materials.[18] The combination of HA improves stiffness, and osteogenic potential in PCL-based scaffolds for bone tissue engineering applications.[19] Moreover, the disadvantages of long absorbable period and acidogenic ability, could be compensated by synchronizing their degradation with that of tri-calcium-phosphate (TCP) and alkaline HA.[20]

At present, there are few researches about the antibacterial properties of PCL/HA scaffolds for bone tissue engineering. ε-Poly-L-lysine (EPL) is naturally occurring homo-polyamide made of 25–35 L-lysine with antimicrobial activities.[21,22] EPL has been used in many novel applications in the fields of food, medicine, environment, agriculture, and electronics because it is biodegradable, water-soluble, thermostable, non-toxic.[23–25] It has a wide antimicrobial spectrum.[26,27] Microorganisms such as bacteria and fungi do not easily develop resistance to this polypeptide.[28]

Although, the preparation and properties of PCL/HA scaffolds have been studied in recent years, there is no report about the improvement of biological and antibacterial properties of 3D printed PCL/HA scaffolds modificated by ε-poly-L-lysine (EPL). The goal of the present study was to produce 3D printed PCL/HA composite scaffolds by the FDM technique and to use EPL to modify the surface of PCL/HA scaffolds, as well to characterize and study the properties of the ε-poly-lysine/polycaprolactone/hydroxyapatite (EPL/HA/PCL) composite scaffolds, which have not been reported in previous studies. Furthermore, the biocompatibility and osteoconductivity of the new composite scaffolds were examined with an osteoblast cell line *in vitro*. Antibacterial annulus was used to observe its antibacterial activity against the *Staphylococcus aureus*, *Escherichia coli* and *Streptococcus mutans*.

2. Materials and methods

2.1 Fabrication of 3D scaffolds

3D printed polycaprolactone (PCL) and polycaprolactone/hydroxyapatite (PCL/HA) scaffolds (Jiangyin Recongene Biomedical Technologies, Ltd Inc., Jiangyin City, China). The PCL, PCL/HA scaffolds were prepared by the FDM technique. The powders of PCL (Shenzhen Esun Industrial Co., Ltd) and HA (Kunshan Overseas Chinese New Material Co., Ltd) particles with sizes ranging from approximately 1 to 20 μm, were mixed with the mass ratio as 7 : 3 in high temperature, then processed as raw materials to produce PCL/HA with the fused deposition modeling (FDM) method. The size of grainy raw materials was less than $2.0 \times 2.0 \times 2.0$ mm^3 by cutting. Scaffolds were fabricated using the FDM 3D modeler system independently developed by manufacturer, with the nozzle diameter of 300 μm. The melting temperature of upper equipment was set at 75 °C and the melting temperature of nozzle tip was maintained at 110 °C during the fabrication process. Aseptic package and cobalt-60 sterilization processing were necessary after the preparation of scaffolds.

2.2 Characterization of scaffolds

2.2.1 Compression testing. Compression testing of PCL and PCL/HA scaffolds was performed based on guidelines for compression testing of acrylic bone cement set in ASTM F451-08.[29,30] $10.0 \times 10.0 \times 5.0$ mm^3 specimens ($n = 5$ for each group) were used for compression tests with a universal materials testing machine (AG-X Plus, Shimadzu Co., Ltd, Shimadzu, Japan). The specimens were compressed at across head speed of 1 mm min^{-1} between two steel platen members.

2.2.2 Surface roughness measurement. The surface roughness of PCL and PCL/HA scaffolds was detected by using a 3D surface profiler based on scanning white light interferometry (Phase shift MicroXAM).

2.2.3 Open porosity of the scaffolds. The open porosity of PCL and PCL/HA scaffolds was tested by the liquid displacement method.[31] The procedure was as follows: firstly, the volume and weight of scaffolds were measured, noted as V and W_0, respectively. Secondly, the samples were immersed into the dehydrated alcohol for 48 h until they were saturated by absorbing dehydrated alcohol, and the samples were weighed again and noted as W_1. Finally, the open porosity of the samples was calculated based on the following formula $P = (W_1 - W_0)/\rho V \times 100\%$, where '$p$' represents the density of dehydrated alcohol. Three samples of each group were analyzed and the mean value of the open porosity of different scaffolds was achieved.

2.2.4 Surface with ε-poly-L-lysine coating. ε-Poly-L-lysine (Zhengzhou Bainafo Bioengineering Co., Ltd). PCL/HA scaffolds were immersed in ε-poly-L-lysine (EPL) water solution (5 mg ml^{-1}). After 24 h, the solution was removed through aspiration, then the PCL/HA scaffolds were dried in vacuum. The above process was repeated three times for subsequent experiments.

2.2.5 Static contact angles. Static contact angles of the scaffolds were measured with a contact angle analyzer (C431, Dataphysics-TP50, Germany) using the sessile drop technique at room temperature. The measurements were carried out in the air, with water being used as the probe liquid. The static contact angle value was the average of five different sites on the scaffolds.

2.2.6 Water uptake capacity. Water uptake was calculated by weighing the scaffolds before and after soaking in distilled water for 2 h. The percent increase in water uptake was calculated as $(\%) = (W_t - W_0)/W_0 \times 100$, where W_t is the weight of the scaffold after 2 h and W_0 is the original weight of the scaffold at time zero. Three samples of each group were measured.

2.2.7 Morphology and pore size of the scaffolds. The morphology of the PCL, PCL/HA and EPL/PCL/HA scaffolds and the pore size of the PCL, PCL/HA scaffolds were observed using scanning electron microscopy (SEM; Hitachi SU8010, Japan). All samples were coated with a conductive layer of sputtered gold before analysis.

2.2.8 The phase and structure. The phase and structure of the scaffolds were characterized by X-ray diffraction (XRD; Shimadzu XRD-7000, Japan) and transform infrared spectroscopy (FT-IR; PerkinElmer, USA). XRD analysis was performed at 4° min^{-1} using Cu target CuKα radiation, a tube voltage 40 kV and a current 30 mA. FT-IR spectra were measured in the

spectral range of 400–4 000 cm^{-1} at different desorption temperatures.

2.2.9 *In vitro* release study. EPL/PCL/HA scaffolds (10.0 × 10.0 × 5.0 mm^3) were used for the vitro release study. Each scaffold was incubated in of phosphate-buffered saline (2.0 ml) at 37 °C under stirring at 60 rpm. At specified time intervals, 0.2 ml of the supernatant was collected, and an equal volume of fresh PBS was added. The content of EPL was measured using a micro BCA protein assay kit according to the manufacturer's instruction. The release profiles were obtained by plotting the percentage of cumulatively content of released EPL against time. The experiments were performed in triplicate.

2.3 Biological compatibility and osteoconductivity

2.3.1 Cell culture. Osteoblast-like cells MC3T3-E1 (Cell Resource Center, Institute of Basic Medical Sciences, Peking Union Medical College, Beijing, People's Republic of China) were cultured in dishes at 37 °C and 100% humidity with 5% CO_2 (volume fraction) in alpha minimum essential medium (Thermo Fisher Scientific, Waltham, MA, USA). The medium was supplemented with 10% volume fraction of fetal bovine serum (Gibco, Rockville, MD) and 1% penicillin/streptomycin (Sigma, St. Louis, MO). Cultures of 90% confluent cells were trypsinized with 2.5 g l^{-1} trypsin containing 1 mmol l^{-1} EDTA (Gibco, Rockville, MD), then washed and suspended in fresh media.

2.3.2 Cell morphology by SEM. Approximately 2 × 10^4 cells were seeded onto each scaffold in alpha minimum essential medium 10% FBS. After 24 h, the cell-scaffold structures were removed from the culture media and washed twice with PBS, fixed with 2.5% glutaraldehyde for 2 h, dehydrated using graded ethanol. Then the samples were coated with platinum and observed under SEM.

2.3.3 Cell proliferation. MC3T3-E1 cells were seeded onto each scaffold in 24-well tissue culture plates (2 × 10^5 cells per well) containing α-MEM medium plus 10% FBS and cultured at 37 °C in a 5% CO_2 humidified incubator. Scaffolds were removed from medium and washed twice with a buffer solution at 1, 3 and 5 days. Cell Counting Kit-8 (CCK-8, Dojindo, Kumamoto, Japan) was used to measure the number of proliferated cells. Briefly, the CCK-8 solution was diluted with culture media (1 : 10 ratio) and then added to each sample. After 4 h incubation, the CCK-8 suspension was extracted and moved to 96-well plates. The optical density (OD) of the extracted suspension was measured at 450 nm using a microplate reader (SpectraMax Paradigm, Austria).

2.3.4 Alkaline phosphatase activity. Scaffolds were put into 24-well plates, then MC3T3-E1 cells were seeded in 24-well plates (2 × 10^5 cells per well) containing α-MEM medium plus 10% FBS. After 24 h, the culture medium was changed to α-MEM, 10% FBS medium and OS containing 10 mmol l^{-1} disodium β-glycerophosphate, 0.15 mmol l^{-1} ascorbic acid and 10^{-8} mol l^{-1} dexamethasone.[32] The medium was changed every 2 days. Scaffolds were removed out of medium and washed twice with buffer solution at 4 and 7 days. Scaffolds were then submerged into 200 μl RIPA lysis buffer solution for cell lysis. Cell lysate was centrifuged and the supernatant was used to calculate alkaline phosphatase (ALP) activity by an ALP activity kit and a BCA assay kit. All results were normalized by protein content.

2.3.5 Alizarin Red staining. MC3T3-E1 cells were seeded in 24-well tissue culture plates (2 × 10^5 cells per well) and cultured overnight at 37 °C in a 5% CO_2 humidified incubator. The medium was then changed to medium containing OS for 19 days. The cells were fixed in 70% ethanol for 1 h at 4 °C. The fixed cells were washed with PBS buffer solution and stained with 1% (w/v) ARS, pH 4.2, for 10 min at room temperature. Then, the formation of mineralized matrix nodules was observed. Scaffolds without cells were used as the blank control group. Quantitative analysis of ARS staining was performed by elution with 10% (w/v) cetylpyridinium chloride for 30 min at room temperature, and the OD value was measured at 562 nm.

2.3.6 RT-qPCR. The osteogenesis-related gene expression levels were quantitatively assessed using RT-PCR for MC3T3-E1 cells cultured on various scaffolds incubated for 7 days. The total RNA of the cells was extracted using TRIzol Reagent (Cwbio), and reverse transcription PCR was performed with the SuperRT cDNA Synthesis Kit (Cwbio) according to the manufacturer's instructions. The expression levels of osteogenic markers were quantified using an UltraSYBR Mixture (Low ROX) (Cwbio). The primer sequences specific for the target gene and the internal control gene (glyceraldehyde-3-phosphate dehydrogenase (GAPDH)) used for qRT-PCR were shown as follows: ALP (F: 5′-GTTGCCAAGCTGGGAAGAACAC-3′; R: 5′-CCCACCCCGCTATTCCAAAC-3′); osteocalcin (F: 5′-CCGGGAGCAGTGTGAGCTTA-3′; R: 5′-AGGCGGTCTTCAAGCCATACT-3′); Runx2 (F: 5′-TTCTCCAACCCACGAATGCAC-3′; R: 5′-CAGGTACGTGTGGTAGTGAGT-3′); GAPDH (F: 5′-GACTTCAACAGCAACTCCCAC-3′; R: 5′-TCCACCACCCTGTTGCTGTA-3′). The RT-qPCR results were analyzed using the $\Delta\Delta C_t$ method and all the data were normalized to GAPDH expression levels.

2.4 Antibacterial activity

Antibacterial activity was determined by the zone of inhibition test using *S. aureus* (Gram-positive bacteria), *E. coli* (Gram-negative bacteria) and *S. mutans* (oral facultative anaerobic bacteria). A microorganism suspension was prepared in 0.9% NaCl in distilled water. Adding microorganism suspension to the prepared agar medium before it solidified. The density of microorganisms in suspension was approximately 10^6 colony-forming units (CFU) per ml for *S. aureus*, 10^5 CFU ml^{-1} for *E. coli*, 10^4 CFU ml^{-1} for *S. mutans*. 13 ml of the agar medium mixed with bacteria was poured into each Petri plate uniformly, then the scaffolds were put into the agar plates. The plates were dried and incubated for 24 h at 37 °C. In the end pictures of all plates were taken using a digital camera.

The killing rate was examined by the viable cell counting technique against *E. coli*. The scaffolds with 15 mm in diameter and 2 mm in height (n = 5 for each group) were immersed in sterilized fluid nutrient medium (5 ml) in test tubes, and 10.0 μl bacterial suspension was inoculated, and cultured at 37 °C. After 24 h, the scaffolds were removed and put into new fluid

nutrient medium, then applied consecutively by the ultrasonic shaking. The surviving bacteria on scaffolds were counted by the spread plate method. After inoculation, the plates were kept at 37 °C and the colonies were counted after 24 h. Efficacy against *E. coli* of the scaffolds was calculated by the following equation: $R = (A - B)/A \times 100\%$, where A is the number of colonies in the PCL/HA group, and B is the number of colonies in the EPL/PCL/HA group (CFU ml^{-1}).

2.5 Statistical analysis

The experiment data have been expressed as the mean ± standard deviation (S.D.). Statistical significance was figured out by means of ANOVA and Student's t test analyses using software spss22.0. The value of $P < 0.05$ was considered statistically significant.

3. Results and discussion

3.1. Characterization of scaffolds

3.1.1 SEM. In low magnification SEM images (Fig. 1a, c and e), the scaffolds showed shifted pattern and regular arrays with interconnected pores. In high magnification SEM images (Fig. 1b, d and f), the fiber of PCL scaffolds had a smooth surface, whereas the fiber of PCL/HA and EPL/PCL/HA scaffolds had a lightly rough surface. Besides the choice of materials, the designability and manufacturability of the structure are both important for scaffolds, so that the scaffolds could not only exhibit the shape-similarity to the physical structure of bone, but also have the internal porous or multi-pipe connected structure that could promote the humoral mobility and cellular adherence.[33,34] In addition, an interconnecting pore network is also essential for tissue ingrowth, vascularization, and nutrient diffusion.[35] The micro-and macroporosity of the scaffolds is supposed to support bone ingrowth, and with an advantage of the induction in cell aggregations that develop along the edges of the scaffolds.[36] Based on SEM images, PCL scaffolds were observed to have a range of channel size 457.98 ± 28.89 μm, filament diameter 304.75 ± 23.14 μm, while PCL/HA scaffolds were observed to have 432.22 ± 32.72 μm and 326.52 ± 31.71 μm respectively. It was reported that pore size of 300–600 μm favors the formation and growth of bone.[37,38] It was clear that the pore sizes of our scaffolds were within the range of favorable sizes for bone regeneration. As a result, the scaffolds prepared in this study could support the formation and growth of bone.

3.1.2 Compressive strength. Fig. 2A showed the stress–strain curves which demonstrate the typical behavior of a honeycomb undergoing deformation.[39] As depicted in Fig. 2B, the compressive modulus of the PCL/HA scaffolds is 49.09 ± 2.615 MPa, while the compressive modulus of the PCL scaffolds is 21.52 ± 1.139 MPa. As a result, compared with PCL scaffolds the compressive modulus of the PCL/HA scaffolds increased 1.28 times. The increased compressive modulus of the PCL/HA scaffolds indicated that mechanical behavior had been improved by adding hydroxyapatite granules. Bone repair scaffolds may bear substantial mechanical stress immediately after implantation. Therefore, the mechanical property of scaffolds should be considered. It has been reported that HA plays the roles of support and filler in bone and can become a part of the bone skeleton.[40] A previous study demonstrated that the HA particles could promote the compressive strength of pure polymeric scaffold.[41] Also, the compressive modulus of cancellous bone was about 10–2000 MPa.[42] The results indicated that PCL/HA scaffolds had a better mechanical capacity to satisfy bone tissue engineering.

3.1.3 Surface roughness, static contact angle, water uptake, and open porosity. Arithmetical average roughness height, as the main indicator of scaffolds surface roughness (Sa), was measured in this study. The results showed that, relative to PCL scaffolds, surface roughness of PCL/HA scaffolds was much

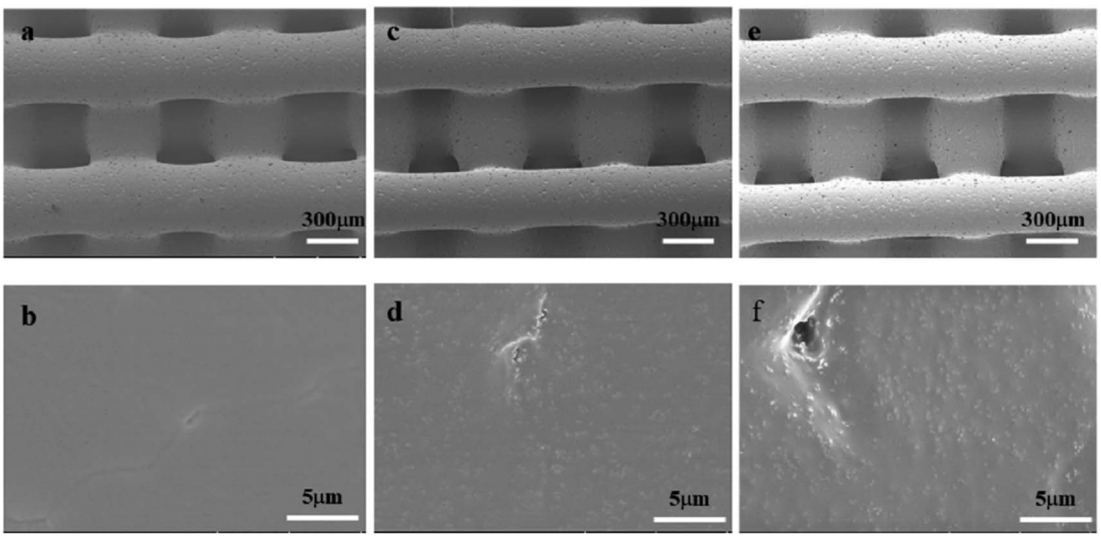

Fig. 1 SEM images: PCL scaffold at 300 μm (a), PCL scaffold at 5 μm (b), PCL/HA scaffold at 300 μm (c), PCL/HA scaffold at 5 μm (d), EPL/PCL/HA scaffold at 300 μm (e), EPL/PCL/HA scaffold at 5 μm (f).

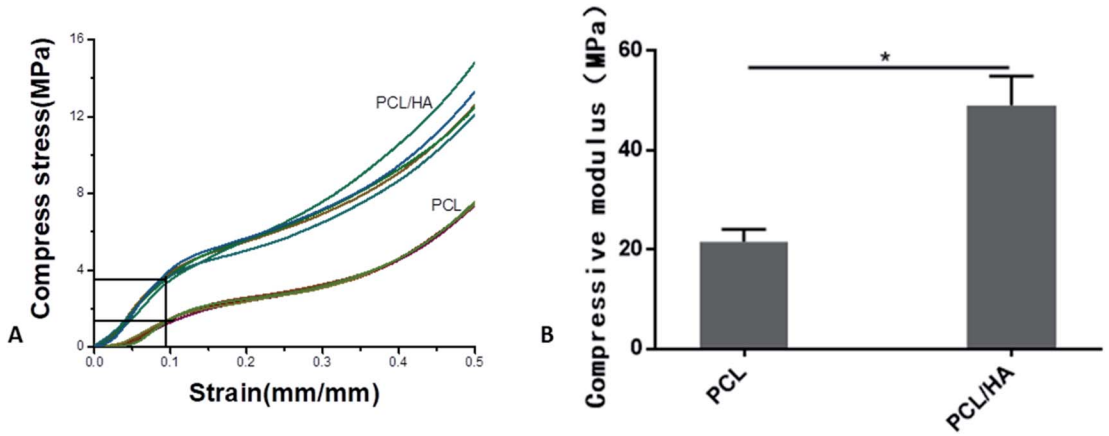

Fig. 2 (A) Stress strain curves of PCL and PCL/HA scaffolds. (B) Compressive modulus of PCL and PCL/HA scaffolds. The data were represented as mean ± standard deviation (SD; $n = 5$; *$p < 0.05$).

rougher (Fig. 3B). The results demonstrated that the scaffolds surface morphology was changed due to adding added HA particles into the polymer. It has been reported that moderately rough surfaces frequently favor the attachment and proliferation of several different cell types compared to smooth surface.[43,44]

The static contact angles of PCL, PCL/HA and EPL/PCL/HA scaffolds were showed in Fig. 3A. The static contact angle of the PCL and PCL/HA scaffolds were 98.08 ± 3.580° and 76.26 ± 2.635° respectively. When PCL/HA scaffolds surface coated by EPL, the contact angle decreased to 37.90 ± 3.087°. Compared to PCL scaffolds, the contact angle of the PCL/HA scaffolds

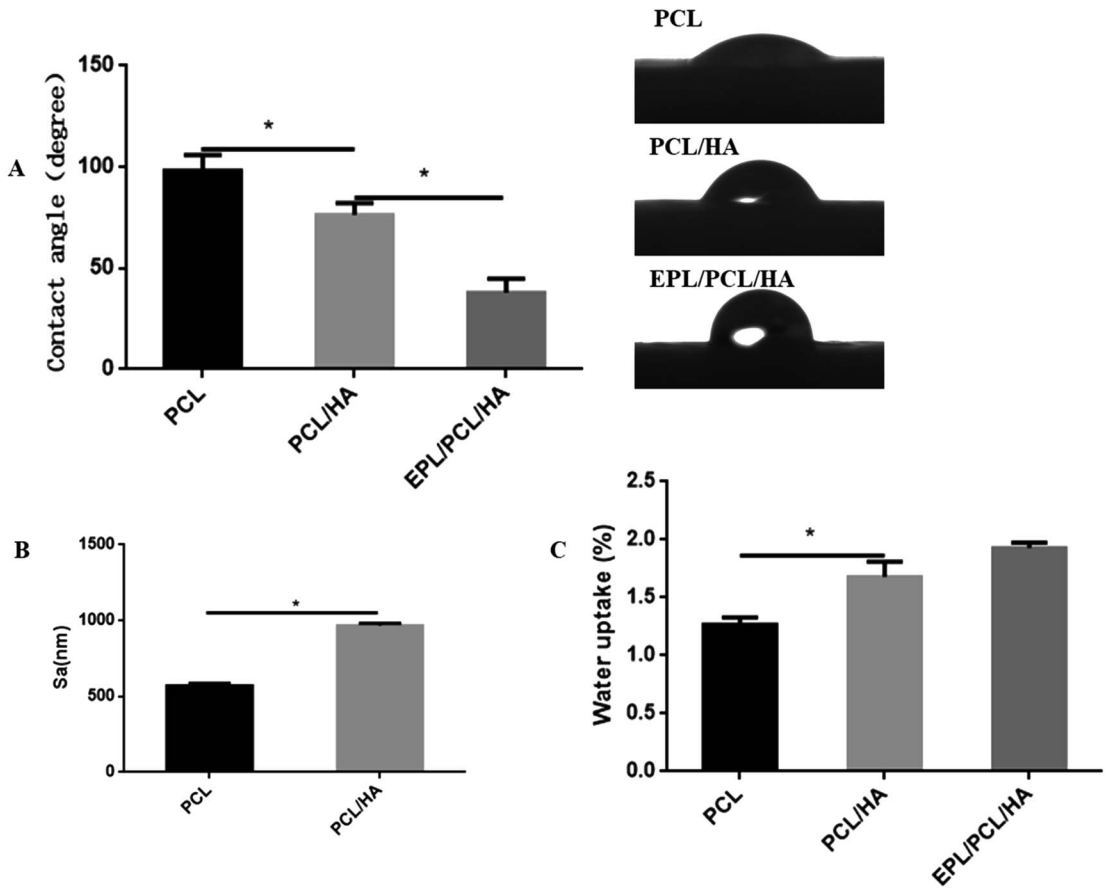

Fig. 3 Contact angle (A), surface roughness (B) and water uptake (C) of PCL, PCL/HA and EPL/PCL/HA scaffolds. Data were presented as mean ± standard deviation. (*$p < 0.05$).

decreased significantly due to the adding of HA particles, while the contact angle of the EPL/PCL/HA scaffolds surface markedly decreased due to EPL coating. A smaller contact angle means a more hydrophilic surface of a material.[45] The results indicated that the hydrophilicity of EPL/PCL/HA scaffolds improved obviously. Fig. 3C showed the differences in water-uptake ability among PCL, PCL/HA and EPL/PCL/HA scaffolds. By adding the HA into PCL scaffolds, the water-uptake ability slightly increased. Furthermore, after EPL was immobilized on the surface of the PCL/HA scaffolds, the water uptake ability of the scaffolds did not significantly increase compared to the PCL/HA scaffolds.

The open porosity of the scaffolds was estimated using liquid displacement method, porosities of the PCL and PCL/HA scaffolds were about 60.25% and 49.05%, respectively, which in the range of the porosity of natural cancellous bone (50–90%).[46]

3.1.4 XRD and FTIR. Fig. 4A showed the comparable XRD patterns of PCL, PCL/HA and HA. The PCL and HA gave typical XRD diffraction patterns. When PCL and HA were mixed, typical PCL and HA peaks were observed, but with decreased peak intensities. In addition, a comparison with the PCL and HA showed no additional peaks in the patterns of the PCL/HA. This indicated that adding HA did not result in a new phase apart from the PCL phase.

The Fourier transform infrared spectroscopy (FTIR) spectra of the EPL/PCL/HA scaffolds clearly showed chemical bands related to pure PCL, HA and EPL (Fig. 4B). There were no significant changes in the band structures when PCL and HA were mixed, suggesting that there was no chemical reaction between PCL and HA in the PCL/HA scaffolds. EPL peaks can be observed in EPL/PCL/HA peaks, which indicated that the EPL existed on the coated surface.

3.1.5 *In vitro* release study. As shown in Fig. 4C, the *in vitro* cumulative release behaviors of EPL from the composites were characterized by the percentage release of EPL as a function of time. A high burst release was noted; more than 80% of the loaded EPL was released within the first 24 h, however it was followed by a slower release over three days. After implanted into body, blood clot would form on the surface of scaffold and inside the interconnected pores which would further improve its slow-release performance.

3.2 Biological compatibility and osteoconductivity

3.2.1 Cell attachment and proliferation. SEM micrographs showed the morphological features of MC3T3-E1 cells cultured on PCL, PCL/HA and EPL/PCL/HA scaffolds for 24 h (Fig. 5). More cells attached on the PCL/HA and EPL/PCL/HA scaffolds surface than on PCL scaffolds surface. Cell–cell interactions were established inside the pores of the PCL/HA and EPL/PCL/HA scaffolds, and this phenomenon was more remarkable on EPL/PCL/HA scaffolds. Excellent cell attachment and extending can be observed on PCL/HA and EPL/PCL/HA scaffolds, while cells had not spread completely on the PCL scaffolds.

The proliferation of MC3T3-E1 cells cultured on PCL, PCL/HA and EPL/PCL/HA scaffolds were assessed using the CCK-8 assay (Fig. 6). The optical density (OD) value of the CCK-8 solution was measured at 1, 3, and 5 days after the cells were seeded. The OD values of the EPL/PCL/HA scaffolds were significantly higher than that of the PCL and PCL/HA scaffolds, and the OD values of PCL/HA scaffolds were much higher than

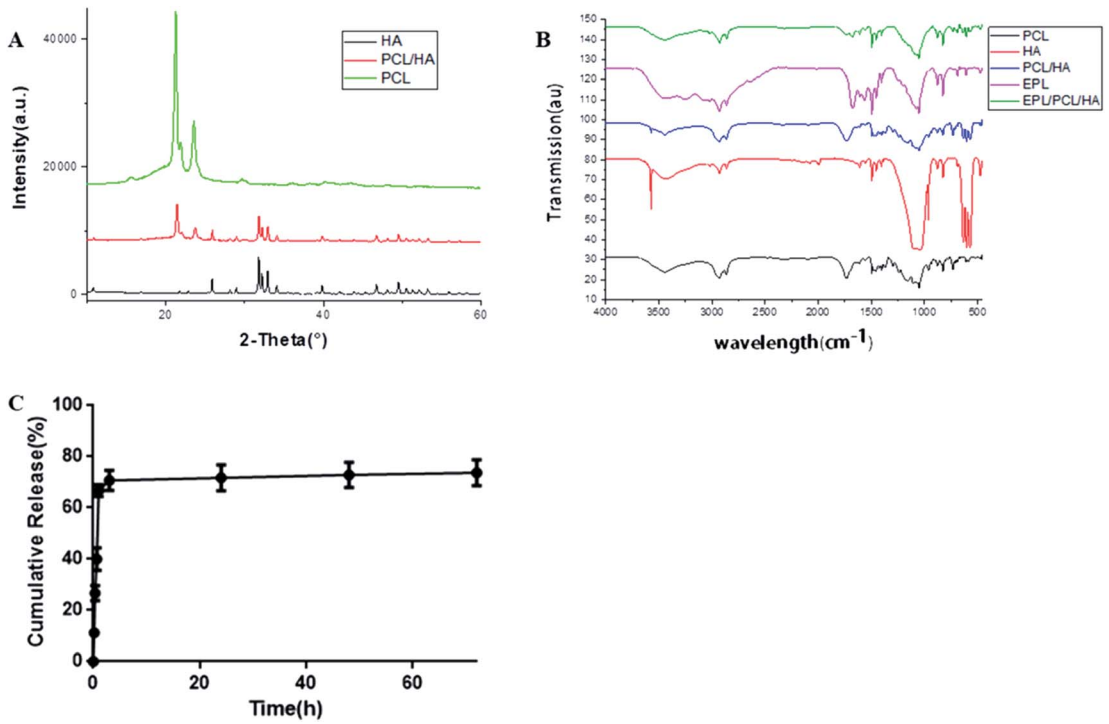

Fig. 4 (A) XRD spectra of HA, PCL and PCL/HA; (B) FT-IR analysis. (C) Release kinetics of EPL from EPL/PCL/HA scaffolds.

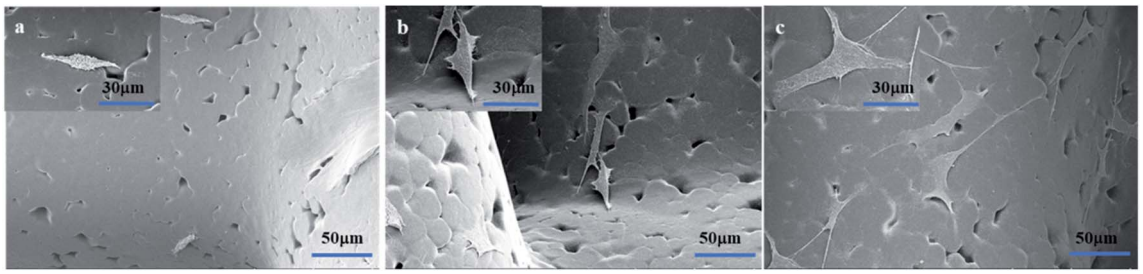

Fig. 5 SEM images of MC3T3-E1 cells on scaffolds ((a) PCL, (b) PCL/HA, (c) EPL/PCL/HA).

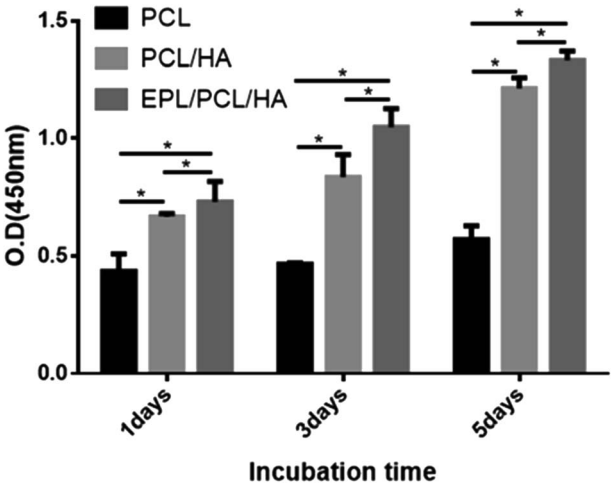

Fig. 6 CCK-8 assay of MC3T3-E1 cells on the scaffolds. Asterisks denote significant differences (*$p < 0.05$).

that of pure PCL scaffolds, which indicated that cell proliferation on the EPL/PCL/HA scaffolds was superior to that on the PCL and PCL/HA scaffolds.

It has been demonstrated that moderately rough surfaces frequently favor the attachment and proliferation of several different cell types compared to smooth surface.[43] Fiber surface roughness can increase the membrane surface area and improve membrane hydrophilicity.[47] In our study, high magnification SEM images (Fig. 1b, d and f) showed that the fibers of PCL/HA and EPL/PCL/HA scaffolds had a moderately rough surface, while the fibers of PCL scaffolds had a smooth surface. Furthermore, the fiber surface roughness of scaffolds was detected by using a 3D surface profiler based on scanning white light interferometry (Fig. 3B), demonstrating the incorporation of HA particles into the polymer resulted in scaffolds with a more heterogeneous morphology and structure. After seeded on scaffolds, MC3T3-E1 cells with longer pseudopodia and processus spread better on PCL/HA and EPL/PCL/HA scaffolds than that on PCL scaffolds (Fig. 5), which in turn demonstrated that moderately rough surfaces of PCL/HA and EPL/PCL/HA scaffolds promoted more cells attachment and proliferation.

Many researchers stated that more hydrophilic than hydrophobic surfaces were better for cell attachment, cell spreading, and cell proliferation.[48] In addition, the hydrophilicity of the material aids in the absorption of fibronectin, which is essential for osteoblast adhesion *in vitro*.[49] Compared to PCL and PCL/HA scaffolds, the static contact angle of the EPL/PCL/HA scaffolds decreased significantly (Fig. 3A). HA can improve the hydrophilicity of polymer material by offering the free –OH group.[50] EPL is a hydrophilic polypeptide, and the amidogens of EPL bound with proteoglycans on the cells' surface facilitate the adhesion effect for cells.[51,52] Therefore, the hydrophilicity of EPL/PCL/HA scaffolds was significantly improved by HA and EPL, which positively affected the behavior of MC3T3-E1 cells. Hence, in our study, results showed EPL/PCL/HA scaffolds were most favourable for cell adhesion and proliferation in three groups.

Lysine residues of EPL coated on the surface of the material with a positive charge could promote the cells adhesion with a negative charge.[53] As a result, after modified by EPL the scaffolds were much more suitable for cells adhesion and proliferation. As shown in photographs (Fig. 5), it was obvious that cytoplasm of MC3T3-E1 cells extended more pseudopodia of filament or sheet shape, and there were more cell–cell interactions inside the pores on EPL/PCL/HA scaffolds than those on PCL/HA scaffolds. What's more, the results of CCK-8 test showed that there was most cells proliferation on EPL/PCL/HA scaffolds.

3.2.2 ALP activity. The appearance of ALP activity is an early phenotypic marker for differentiation of osteoblasts.[54] The ALP expression is associated with formation of osteoprogenitors that proliferate and differentiate into identifiable osteoblasts, bone lining cells, and finally, to a new bone formation.[55] In the presence of osteogenic stimulation, cells on EPL/PCL/HA scaffolds had higher bioactivity of alkaline phosphatase at 4 days and 7 days compared with on the PCL/HA scaffolds and PCL scaffolds (Fig. 7). The PCL scaffolds presented the lowest differentiation potential (Fig. 7). It was obvious that the addition of HA particles enhanced the osteogenic properties of scaffolds, while osteoblastic potentials of PCL/HA scaffolds was further improved after coated by EPL. Results revealed that EPL/PCL/HA scaffolds were more favorable to the expression of alkaline phosphatase, which was important for osteogenesis.

3.2.3 Alizarin Red staining. Mineralized nodule formation is a phenotypic marker for the last stage of mature osteoblasts.[54] After incubation of MC3T3-E1/scaffold composite in OS for 19 days, more obvious positive staining of Alizarin Red S (RAS) on PCL/HA and EPL/PCL/HA scaffolds (Fig. 8B(b and c)) was

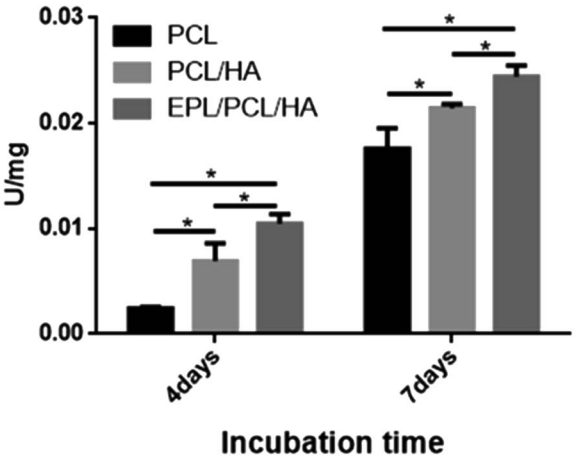

Fig. 7 ALP activity of MC3T3-E1 cells on the scaffolds. Asterisks denote significant differences (*$p < 0.05$).

observed than that on PCL scaffolds (Fig. 8B(a)). Alizarin Red staining and quantitative analyses (Fig. 8C) suggested that mineralization of PCL and PCL/HA scaffolds was significantly lower than that of EPL/PCL/HA scaffolds, and mineralization of PCL scaffolds was significantly lower than that of PCL/HA scaffolds. The results of Alizarin Red staining of PCL, PCL/HA and EPL/PCL/HA scaffolds were in complete agreement with the trends obtained for cells proliferation and differentiation by CCK-8 and ALP assay on these scaffolds. Furthermore, the results of Alizarin Red staining had clearly indicated that the osteogenetic properties of the scaffolds were influenced significantly by the EPL coating on PCL/HA scaffolds.

3.2.4 RT-PCR. Expression of genes involved with osteogenesis (ALP, Runx2 and Osteocalcin) was further determined by performing real-time quantitative RT-PCR on the cells cultured for 7 days. As shown in Fig. 9, for ALP, Runx2 and Osteocalcin (OCN) gene expression, upregulation was observed in the EPL/PCL/HA and PCL/HA scaffolds when compared to the PCL scaffolds. ALP, Runx2 and OCN gene expression changes were insignificant in the EPL/PCL/HA scaffolds when compared to the PCL/HA scaffolds.

No bone formation was observed in Runx2 null mice,[56] suggesting that Runx2 is a key transcription factor for osteoblast differentiation.[57] ALP is considered to play an important role in the process of mineral formation in tissues like bone, cartilage tooth root cementum and dentin.[58] Osteocalcin (OCN) is expressed during the postproliferative period and reaches its maximum expression during mineralization and accumulates in the mineralized bone.[59] The conclusion can be drawn that the addition of the HA particles in this study induced the high expression of ALP, Runx2 and OCN in MC3T3-E1 cells cultured on EPL/PCL/HA and PCL/HA scaffolds, and in turn promoted the process of osteoblast differentiation and bone formation. The ability of HA in composite materials to stimulate osteogenesis had been reported in several studies.[60,61] Research suggests that HA powder particle size can contribute to modulation of osteoblast gene expression.[62] Besides, the moderately rough surface of scaffolds may promote the osteogenic differentiation of MC3T3-E1. Studies show that moderately rough surface of materials have the potential to promote expression of the osteogenic and osteogenic differentiation of human bone marrow-derived mesenchymal stromal cells (hMSCs).[63] The results had proved that EPL/PCL/HA and PCL/HA scaffolds had moderately rough surface which also could cause the high osteogenic differentiation and more mineralization. On the other hand, our results showed that EPL/PCL/HA scaffolds had higher ALP activity (Fig. 7) and more mineralization in Alizarin Red staining and quantitative analysis (Fig. 8) than PCL/HA scaffolds, while there was no significant difference between the expressions of the osteogenesis-related genes of the EPL/PCL/HA scaffolds and that of the PCL/HA scaffolds. This may result from more MC3T3-E1 cells can adhere and proliferate on EPL/PCL/HA scaffolds due to EPL modification.

3.3 Antibacterial activity

Images of agar plates antimicrobial assay results were showed in Fig. 10. After 24 hours incubation, a transparent zone was

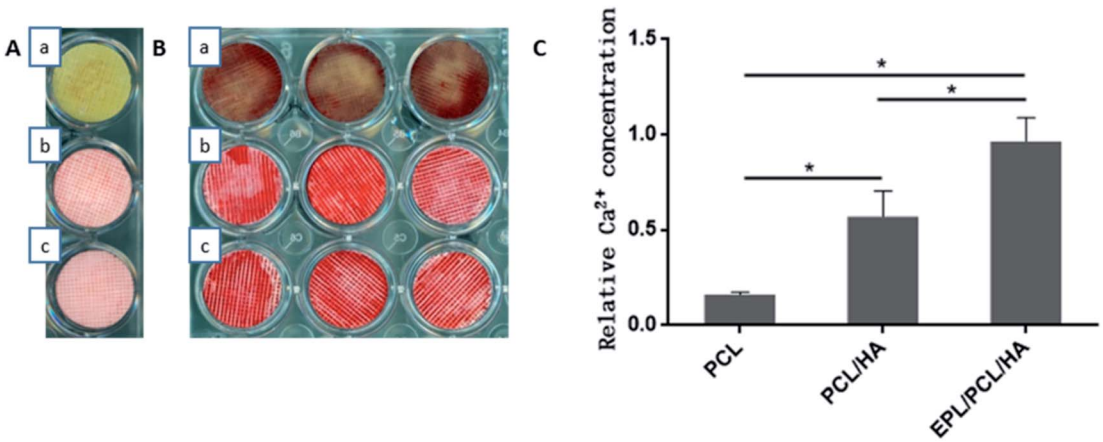

Fig. 8 (A) Alizarin Red S staining of scaffolds without MC3T3-E1 cells ((a) PCL, (b) PCL/HA, (c) EPL/PCL/HA), (B) Alizarin Red S staining of MC3T3-E1 cells on the scaffolds ((a) PCL, (b) PCL/HA, (c) EPL/PCL/HA); (C) ARS quantification of mineral content.

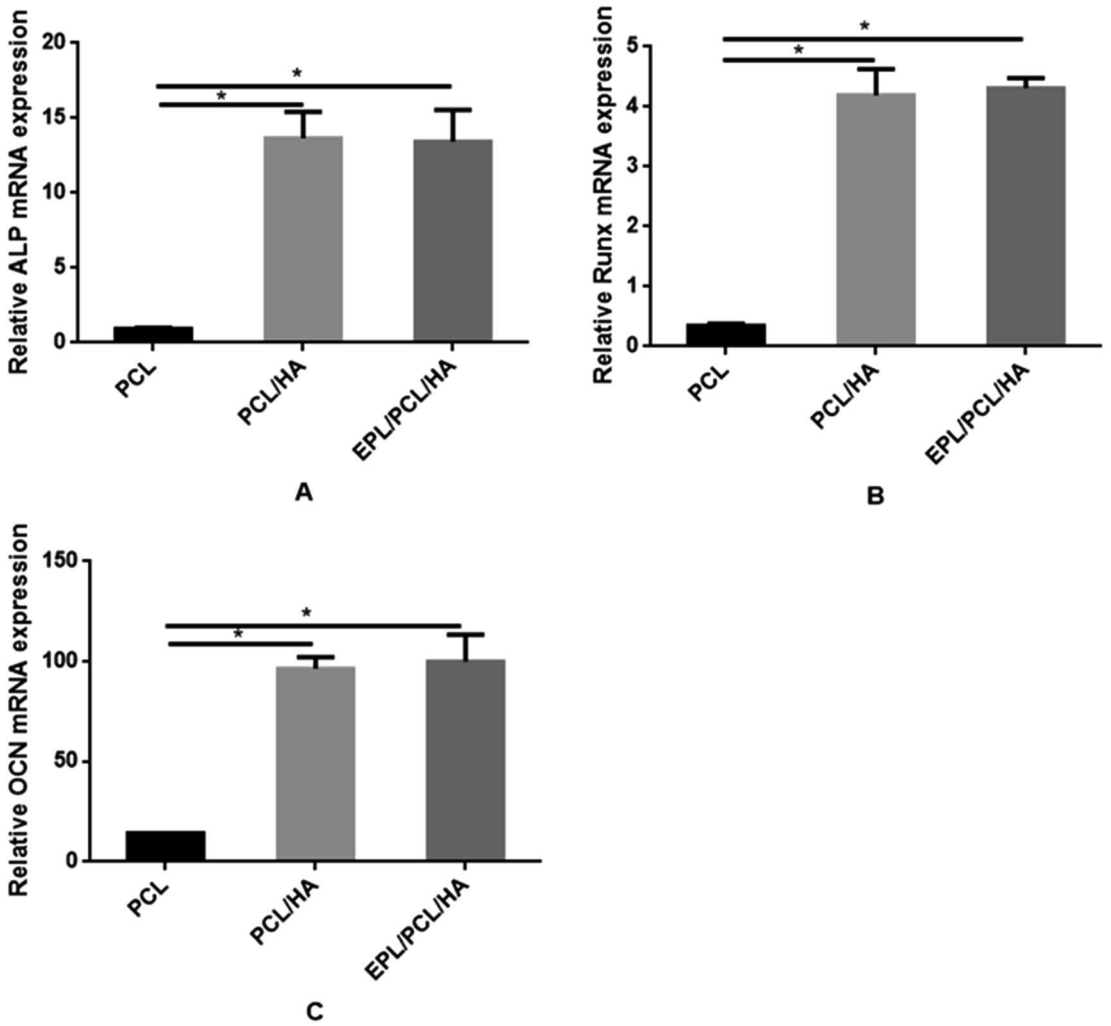

Fig. 9 Quantitative analyses of osteogenesis-related gene expressions (*i.e.*, ALP (A), Runx2 (B) and OCN (C)). The data were represented as mean ± standard deviation ($n = 3$; $^*p < 0.05$).

observed around the EPL/PCL/HA scaffolds (Fig. 10(Ac, Bc and Cc)), in contrast to the opaque parts over the zone where bacteria were alive. While there was no transparent inhibition zone around the PCL and PCL/HA scaffolds (Fig. 10(Aa, Ab, Ba, Bb, Ca and Cb)). The antibacterial effect did not obviously change after subsequent culture for 3 days (Fig. 10(Af, Bf and Cf)). It turned out to be that the EPL/PCL/HA scaffolds composite exhibited an excellent broad-spectrum antibacterial activities against *S. aureus*, *E. coli* and *S. mutans in vitro*, and the antimicrobial activity of EPL/PCL/HA scaffolds was retained for an extended time period. When PCL and PCL/HA scaffolds were taken as control samples, antibacterial rate of EPL/PCL/HA scaffolds against *E. coli* was 92.42%. The antimicrobial nature of any implanted graft material aids in the persistence of the implant by preventing microbial attacks associated with surgeries. In our case, we used EPL to modify the surface of PCL/HA scaffold, to obtain a bone tissue engineering scaffold with antibacterial property. ε-Poly-L-lysine (EPL) is a linear L-lysine homopolymer biosynthesized by actinomyces, and it has a unique structure linking ε-amino and α-carboxylic acid functional groups,[64] known to have a broad-spectrum antibacterial activity against Gram-positive and Gram-negative bacteria.[65] The mechanism of inhibited microbial growth was studied and concluded that the electrostatic adsorption of EPL to the cell surface followed by the stripping of the outer membrane and abnormal distribution of the cytoplasm ultimately led to physiological damage of the EPL treated microbes.[26] Marian Fürsatz *et al.*, evaluated the biopolymer of EPL functionalized bacterial cellulose (BC) *in vitro* and had demonstrated that polymer exhibited efficient contact inhibition of *S. epidermidis* and did not affect the cytocompatibility to cultured human fibroblasts.[66] In our study, FITR exam proved the existence of EPL in composite scaffolds and no chemical reaction produced among EPL, HA and PCL, illustrating that chemical property of EPL did not change. In summary, EPL is a promising, green and versatile modified material to improve the performance of 3D-printed PCL/HA scaffolds for the earlier period of bone formation.

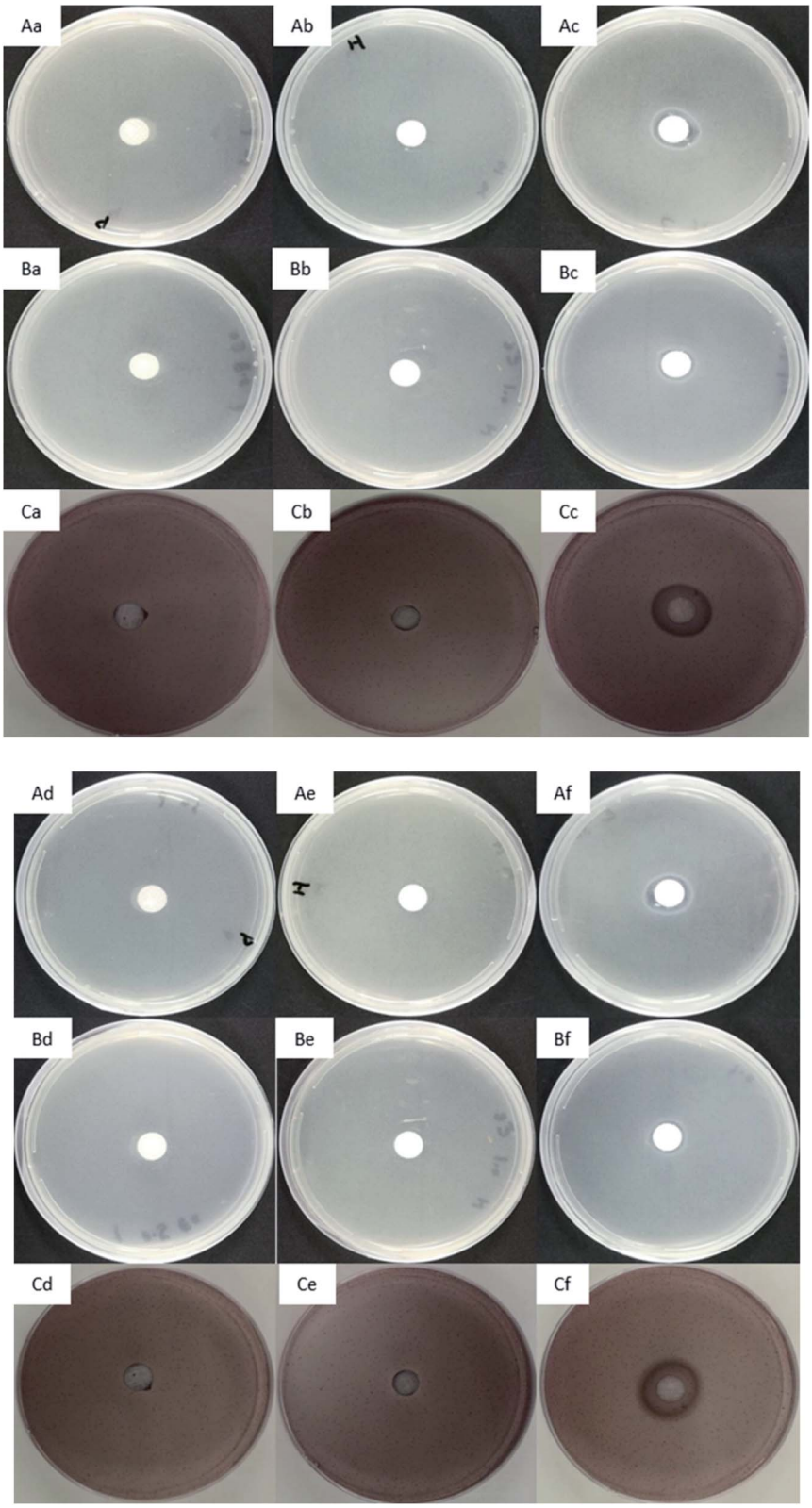

Fig. 10 Antimicrobial effect of scaffolds on *S. aureus* (A), *E. coli* (B) and *S. mutans* (C); bacteria cultures after 24 hours: PCL scaffolds (Aa, Ba and Ca), PCL/HA scaffolds (Ab, Bb and Cb), EPL/PCL/HA scaffolds (Ac, Bc and Cc); subsequent culture for 3 days: PCL scaffolds (Ad, Bd and Cd), PCL/HA scaffolds (Ae, Be and Ce), EPL/PCL/HA scaffolds (Af, Bf and Cf).

4. Conclusions

In this study, 3D printed PCL/HA scaffold has been modified using ε-poly-L-lysine (EPL) to build a new EPL/HA/PCL composite scaffold for infection prevention and better bone formation in patient-specific bone defect treatments. The created scaffolds were found to be cytocompatible as well as capable of osteogenic differentiation and antimicrobial activity *in vitro*, which is beneficial not only to bone regeneration, but to reduce or prevent the incidence of the infective complications in reparative bone formation. Further investigations are needed to determine if the present scaffolds can support functional tissue regeneration *in vivo*.

Conflicts of interest

There are no conflicts to declare.

Acknowledgements

This work was financially supported by the Natural Science Foundation of China (81171004 and 81300916).

References

1 C. Myeroff and M. Archdeacon, *J. Bone Jt. Surg., Am. Vol.*, 2011, **93**, 2227–2236.
2 C. Lakhiani, M. V. DeFazio, K. Han, R. Falola and K. Evans, *J. Reconstr. Microsurg.*, 2016, **32**, 342–357.
3 P. Li, Q. Fang, J. Qi, R. Luo and C. Sun, *J. Oral Maxillofac. Surg.*, 2015, **73**, 1637–1640.
4 J. M. Toto, E. I. Chang, R. Agag, K. Devarajan, S. A. Patel and N. S. Topham, *Head & Neck*, 2015, **37**, 1660–1664.
5 S. J. Heo, S. E. Kim, J. Wei, Y. T. Hyun, H. S. Yun, D. H. Kim, J. W. Shin and J. W. Shin, *J. Biomed. Mater. Res., Part A*, 2009, **89**, 108–116.
6 X. Y. Zhang, G. Fang and J. Zhou, *Materials*, 2017, **10**, 50.
7 J. M. Sobral, S. G. Caridade, R. A. Sousa, J. F. Mano and R. L. Reis, *Acta Biomater.*, 2011, **7**, 1009–1018.
8 J. Y. Lee, B. Choi, B. Wu and M. Lee, *Biofabrication*, 2013, **5**, 045003.
9 S. A. Park, S. H. Lee and W. D. Kim, *Bioprocess Biosyst. Eng.*, 2011, **34**, 505–513.
10 M. Nikzad, S. H. Masood and I. Sbarski, *Mater. Des.*, 2011, **32**, 3448–3456.
11 C. X. Lam, D. W. Hutmacher, J. T. Schantz, M. A. Woodruff and S. H. Teoh, *J. Biomed. Mater. Res., Part A*, 2009, **90**, 906–919.
12 M. A. Woodruff and D. W. Hutmacher, *Prog. Polym. Sci.*, 2010, **35**, 1217–1256.
13 S. Eshraghi and S. Das, *Acta Biomater.*, 2010, **6**, 2467–2476.
14 G. L. Siparsky, K. J. Voorhees and F. D. Miao, *J. Environ. Polym. Degrad.*, 1998, **6**, 31–41.
15 O. M. Bostman, *J. Bone Jt. Surg. Br. Vol.*, 1991, **73**, 679–682.
16 H. Zhou and J. Lee, *Acta Biomater.*, 2011, **7**, 2769–2781.
17 A. Azari, S. Nikzad, A. Yazdani, F. Atri and A. F. Anvari-Yazdi, *J. Mater. Sci.: Mater. Med.*, 2017, **28**, 111.
18 M. Okamoto and B. John, *Prog. Polym. Sci.*, 2013, **38**, 1487–1503.
19 N. Koupaei and A. Karkhaneh, *J. Tissue Eng. Regener. Med.*, 2016, **13**, 251–260.
20 V. Uskokovic and D. P. Uskokovic, *J. Biomed. Mater. Res., Part B*, 2011, **96**, 152–191.
21 S. Shima and H. Sakai, *Agric. Biol. Chem.*, 2014, **45**, 2497–2502.
22 S. Shima and H. Sakai, *Agric. Biol. Chem.*, 2014, **45**, 2503–2508.
23 A. H. Chheda and M. R. Vernekar, *Int. Food Res. J.*, 2015, **22**, 23–30.
24 M. Laura, M. Núria, F. Vicente, d. l. T. Cristina, A. Alessandro, M.-M. e. Ramón, S. Félix, A. Pedro, P.-P. Enrique and O. Mar, *Chemistry*, 2014, **20**, 5271–5281.
25 H. Mandal, S. S. Katiyar, R. Swami, V. Kushwah, P. B. Katare, A. M. Kumar, S. K. Banerjee, A. Popat and S. Jain, *Int. J. Pharm.*, 2018, **542**, 142–152.
26 S. Shima, *J. Antibiot.*, 1984, **37**, 1449–1455.
27 A. K. Pandey and A. Kumar, *Process Biochem.*, 2014, **49**, 496–505.
28 H. Gao and S.-Z. Luo, *RSC Adv.*, 2016, **6**, 58521–58528.
29 M. E. Hoque, D. W. Hutmacher, W. Feng, S. Li, M. H. Huang, M. Vert and Y. S. Wong, *J. Biomater. Sci., Polym. Ed.*, 2005, **16**, 1595–1610.
30 D. W. Hutmacher, T. Schantz, I. Zein, K. W. Ng, S. H. Teoh and K. C. Tan, *J. Biomed. Mater. Res.*, 2001, **55**, 203–216.
31 J. Venkatesan, Z.-J. Qian, B. Ryu, N. Ashok Kumar and S.-K. Kim, *Carbohydr. Polym.*, 2011, **83**, 569–577.
32 D. D. Liu, J. C. Zhang, C. Q. Yi and M. S. Yang, *Sci. Bull.*, 2010, **55**, 1013–1019.
33 I. H. Pereira, E. Ayres, L. Averous, G. Schlatter, A. Hebraud, A. C. de Paula, P. H. Viana, A. M. Goes and R. L. Oréfice, *J. Mater. Sci.: Mater. Med.*, 2014, **25**, 1137–1148.
34 Q. Yao, B. Wei, Y. Guo, C. Jin, X. Du, C. Yan, J. Yan, W. Hu, Y. Xu, Z. Zhou, Y. Wang and L. Wang, *J. Mater. Sci.: Mater. Med.*, 2015, **26**, 5360.
35 J. Lee, M. J. Cuddihy and N. A. Kotov, *Tissue Eng., Part B*, 2008, **14**, 61.
36 H. Seitz, W. Rieder, S. Irsen, B. Leukers and C. Tille, *J. Biomed. Mater. Res., Part B*, 2005, **74**, 782–788.
37 C. M. Murphy, M. G. Haugh and F. J. O'Brien, *Biomaterials*, 2010, **31**, 461–466.
38 I. Martin, R. F. Padera, G. Vunjaknovakovic and L. E. Freed, *J. Orthop. Res.*, 1998, **16**, 181.
39 S. Nguyen and R. H. Marchessault, *J. Biomed. Mater. Res., Part B*, 2006, **77**, 5.
40 G. V. Salmoria, E. A. Fancello, C. R. M. Roesler and F. Dabbas, *Int. J. Adv. Manuf. Technol.*, 2013, **65**, 1529–1534.
41 O. Y. Alothman, F. N. Almajhdi and H. Fouad, *Biomed. Eng. Online*, 2013, **12**, 95.
42 T. Almela, I. M. Brook, K. Khoshroo, M. Rasoulianboroujeni, F. Fahimipour, M. Tahriri, E. Dashtimoghadam, A. El-Awa, L. Tayebi and K. Moharamzadeh, *Bioprinting*, 2017, **4**, 1.
43 J. H. Shim, J. B. Huh, Y. P. Ju, Y. C. Jeon, S. S. Kang, J. Y. Kim, J. W. Rhie and D. W. Cho, *Tissue Eng., Part A*, 2013, **19**, 317–328.

44 A. Itälä, H. O. Ylänen, J. Yrjans, T. Heino, T. Hentunen, M. Hupa and H. T. Aro, *J. Biomed. Mater. Res.*, 2002, **62**, 404–411.
45 Y. Yang, X. Ding, T. Zou, G. Peng, H. Liu and Y. Fan, *RSC Adv.*, 2017, **7**, 7954–7963.
46 L. A. Di, A. Longoni, G. Criscenti, C. Mota, B. C. Van and L. Moroni, *Biofabrication*, 2016, **8**, 045007.
47 Q. Liu, Y. F. Song, B. Grottkau, M. X. Ma, C. Ye and B. Guo, *BioMed Res. Int.*, 2017, **2017**, 1–12.
48 J. Wei, M. Yoshinari, S. Takemoto, M. Hattori, E. Kawada, B. Liu and Y. Oda, *J. Biomed. Mater. Res., Part B*, 2007, **81**, 66–75.
49 M. Yang, S. Zhu, Y. Chen, Z. Chang, G. Chen, Y. Gong, N. Zhao and X. Zhang, *Biomaterials*, 2004, **25**, 1365–1373.
50 S. Dhivya, S. Saravanan, T. P. Sastry and N. Selvamurugan, *J. Nanobiotechnol.*, 2015, **13**, 40.
51 L. Qian and W. M. Saltzman, *Biomaterials*, 2004, **25**, 1331–1337.
52 Y. E. Qing, K. Chen, W. U. Huang, H. E. Yunsong, M. Nong, L. I. Chunxiang and T. Liang, *Exp. Ther. Med.*, 2015, **9**, 25–32.
53 C. R. Wittmer, J. A. Phelps, W. M. Saltzman and P. R. Van Tassel, *Biomaterials*, 2007, **28**, 851–860.
54 Y. F. Chou, J. C. Dunn and B. M. Wu, *J. Biomed. Mater. Res., Part B*, 2005, **75**, 81–90.
55 S. Kwak, A. Haider, K. C. Gupta, S. Kim and I. K. Kang, *Nanoscale Res. Lett.*, 2016, **11**, 323.
56 T. Komori, H. Yagi, S. Nomura, A. Yamaguchi, K. Sasaki, K. Deguchi, Y. Shimizu, R. T. Bronson, Y. H. Gao and M. Inada, *Cell*, 1997, **89**, 755–764.
57 Z. Maruyama, C. A. Yoshida, T. Furuichi, N. Amizuka, M. Ito, R. Fukuyama, T. Miyazaki, H. Kitaura, K. Nakamura and T. Fujita, *Dev. Dyn.*, 2010, **236**, 1876–1890.
58 G. Harrison, I. M. Shapiro and E. E. Golub, *J. Bone Miner. Res.*, 2010, **10**, 568–573.
59 D. Liu, J. Zhang, Y. Li, S. Wang and M. Yang, *Biol. Trace Elem. Res.*, 2012, **149**, 291–297.
60 M. E. Frohbergh, A. Katsman, M. J. Mondrinos, C. T. Stabler, K. D. Hankenson, J. T. Oristaglio and P. I. Lelkes, *Tissue Eng., Part A*, 2015, **21**, 970.
61 X. Liu, L. A. Smith, J. Hu and P. X. Ma, *Biomaterials*, 2009, **30**, 2252–2258.
62 J. Xie, M. J. Baumann and L. R. McCabe, *J. Biomed. Mater. Res., Part A*, 2004, **71**, 108–117.
63 I. Wall, N. Donos, K. Carlqvist, F. Jones and P. Brett, *Bone*, 2009, **45**, 17–26.
64 T. Bo, P. P. Han, Q. Z. Su, P. Fu, F. Z. Guo, Z. X. Zheng, Z. L. Tan, C. Zhong and S. R. Jia, *Food Control*, 2015, 7135.
65 R. Ye, H. Xu, C. Wan, S. Peng, L. Wang, H. Xu, Z. P. Aguilar, Y. Xiong, Z. Zeng and H. Wei, *Biochem. Biophys. Res. Commun.*, 2013, **439**, 148–153.
66 M. Fürsatz, M. Skog, P. Sivler, E. Palm, C. Aronsson, A. Skallberg, G. Greczynski, H. Khalaf, T. Bengtsson and D. Aili, *Biomed. Mater.*, 2018, **13**, 025014.

